

UNIVERSITY ULM

MASTER THESIS

Optical Properties of Colour Centres in Nanodiamonds

Author:
Ou Wang

Supervisor:
Prof. Fedor Jelezko
Prof. Ute Kaiser

*A thesis submitted in partial fulfillment of the requirements
for the degree of Master of Science*

in the

Institute of Quantum Optics
Department of Science

October 10, 2016

Declaration of Authorship

I, Ou Wang, declare that this thesis titled, "Optical Properties of Colour Centres in Nanodiamonds" and the work presented in it are my own. I confirm that:

- This work was done wholly or mainly while in candidature for a research degree at this University.
- Where any part of this thesis has previously been submitted for a degree or any other qualification at this University or any other institution, this has been clearly stated.
- Where I have consulted the published work of others, this is always clearly attributed.
- Where I have quoted from the work of others, the source is always given. With the exception of such quotations, this thesis is entirely my own work.
- I have acknowledged all main sources of help.
- Where the thesis is based on work done by myself jointly with others, I have made clear exactly what was done by others and what I have contributed myself.

Signed:

Date:

UNIVERSITY ULM

Abstract

Quantum Optics
Department of Science

Master of Science

Optical Properties of Colour Centres in Nanodiamonds

by Ou WANG

Contents

Declaration of Authorship	iii
1 Motivation and Background	1
1.1 Quantum information processing and Qubit candidates	1
1.2 Silicon vacancy as a Qubit candidate	2
1.3 Silicon vacancies in nanodiamonds	3
1.4 Motivation of the thesis	4
2 Sample preparation and Experiment Apparatus	7
2.1 Sample information	7
2.2 sample preparation	8
2.2.1 preparation of the substrate	8
2.2.2 spin-coating of the sample	9
spin-coating theory	9
Acid cleaning	10
spin-coating practice	10
2.3 experiment apparatus	11
The initial Setup	11
Methods for characterisation	12
3 Surface treatments	17
3.1 Oxidation	17
3.1.1 first Oxidation	17
3.1.2 Second Oxidation	20
3.2 H termination	22
4 Result and Discussion	25
4.1 Compilation of data	25
4.2 Nanodiamond size and spectral stability	25
4.3 Excitation power and spectral stability	26
4.4 Temperature and spectral stability	27
4.5 Excitation polarisation and spectral stability	27
4.6 Aerobic Oxidation and Spectral stability	28
4.7 Hydrogen termination	28
5 Conclusion and outlook	35
5.1 The road so far	35
5.2 Probabilities in the near future	35
A Appendix Title Here	37

Chapter 1

Motivation and Background

1.1 Quantum information processing and Qubit candidates

The bit is the basic unit of information in computing and digital communications. A bit can have one value, which can be 1 or 0, that represents the logical states in a 2-level logic system. In modern digital computers, these two states exists as low and high voltages in highly integrated circuits. Just like a bit for classical computing, a qubit is the basic unit of information in Quantum Information Processing (QIP), which encodes 1 and 0 into 2 distinguishable quantum states. As the qubits behave in the manner of quantum mechanism, it gives rise to the phenomena of superposition and entanglement, the computing power increases exponentially while more qubits adding up together. Previous difficult tasks in classical computing such as simulation of quantum systems or factoring of numbers would be finished quickly and efficiently by quantum computers.

For the realisation of quantum computer, the first priority is to find a fitting candidate as qubit. Five principles have been brought up for the candidates choosing by [DiVincenzo,2000]:

1. A scalable physical system with well characterized qubits
2. The ability to initialize the state of qubits to a simple fiducial state
3. Long relevant decoherence times, much longer than gate operation time
4. A "universal" set of quantum gates
5. A qubit-specific measurement capability

Color centres are optically active impurities that are responsible for the colors in crystals that are transparent due to large band gap. They are atom-like solid systems that, with appropriate electronic structure and symmetry in crystal, can be the candidates for qubits. Additionally, it is practical to require a long enough coherent time for the operations and for the readout.

Lots of research has been done with the negative charged nitrogen vacancy (NV^-), which has excellent spin properties at ambient condition, it has also been proved that it is possible to execute an all optical access to its spin.[reference from all optical paper]. Yet due to the transform of symmetry during the excitation process, NV^- has a big phonon side band following the zero-phonon line (ZPL). Moreover, the C3v symmetry leaves the color centre vulnerable towards the environment electric field, resulting in spectral diffusion, which is caused by the flipping of charging state. These disadvantages has reduced the generation rate of coherent photon generation rates and limit the development of NV-quantum networks[Lachlan paper].

1.2 Silicon vacancy as a Qubit candidate

Negative charged Silicon vacancy centres (SiV^-) are considered as the next promising qubit candidate after NV^- . It has irresistibly excellent optical properties, and is also possible to achieve an all optical initializaiton, read out and coherent preparation.

SiV^- has a D_{3d} symmetry with the symmetry axis along the $\langle 111 \rangle$ crystal direction. The color center consists of a substital Silicon atom and a carbon vacancy. Due to the size difference between Silicon atoms and carbon atoms, it is expected that the Silicon atom will sit between 2 lattice site instead of on a lattice site[Goss etal, Gali and Maze,]. The inversion symmetry offers SiV^- extra shielding from the small electric field fluctuation.

Experimentally it is observed that the SiV^- has outstanding optical properties, 70% of its fluorescence couples into a sharp ZPL of 1.68eV. At cryogenic temperature this ZPL can be resolved with a fine structure of 4 lines. These four lines are signed to the electronic transitions between the ground state and the first excited state of SiV^- . Theoretical calculation based on the group theory and ab initio method offers us a model of the SiV^- electronic structure with a ground state of 2 folded degeneracy and even parity, a first excited state of 2 folded degeneracy of uneven parity and a second excited state of none degeneracy with even parity.[Goss etal] This calculation fits the observation as only the electronic transition between levels of different parity is allowed, due to the -1 parity of photons, thus only the 4 transitions between the first excited state and the ground state would be allowed, as signed to the 4 line structure of ZPL. Since this is a E to E transition, no dramatic symmetry change has been involved, less phonon would be involved in the relaxation, which fits the observation of the sharp ZPL with small phonon side band.

Lachlan et al showed the probility to read out and coherently prepare electronic spin in individual SiV^- centers via resonance excitation. The SiV^- was first initialized by resonantly pumping the spin-flipping transition D1 that is weakly allowed due to the off axis residue of the magnetic field, this is done with applying a laser pulse that resonant to transition D1. After a dark interval the spin state was read out using a laser pulse on the cycling transition D2. The leading edge peak from D2 pulse will decrease with the increase of dark interval approaching an minimum. From which the spin relaxation time T1 has be calculated as $2.4 \pm 0.2\text{ms}$. With the similar pulse measurement, the orbital T1 has been measured as $38 \pm 1\text{ns}$. The fact that the orbital T1 is much shorter than spin T1 indicates that the orbital relaxation is highly spin conserving, as the electron phonon interaction should be. The temperature dependency measurement reveals that the orbital rate increase linear with the temperature until 22K, which indicates a single-phonon mechanism of orbital relaxation.[Lachlan et al, and 30-32 from the paper]

Further CPT was carried out by tuning the pump laser to transition D2 while scanning across the transition D1 using the probe laser. The spin coherent time was then measured to be $35 \pm 3\text{ns}$. This short coherence time is likely to be connected to the dephasing caused by the rapid orbital relaxation.

Practically, as mention before, a qubit candidate ideally need to have long enough coherent time for the implementation of operation and read

out, in this sense, the short coherent time of SiV^- drew it back from being an competitive qubit candidate.

Several ideas of acquiring longer coherence time has been taken into consideration. While most of them can be classified into two main approaches: avoid orbital relaxation caused electron spin dephasing by accessing the orbital spin in Si^{29} or eliminate the single phonon that has been involved in the orbital relaxation.

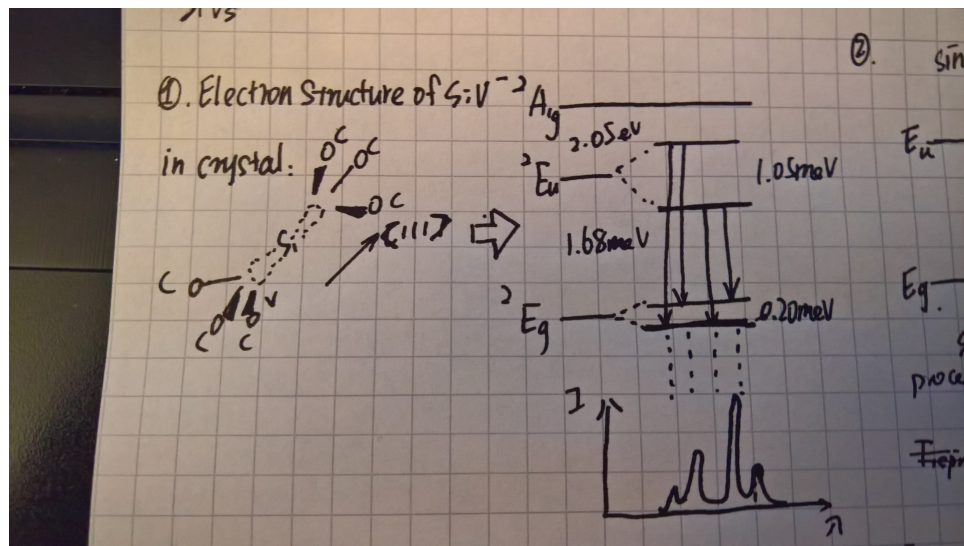


FIGURE 1.1

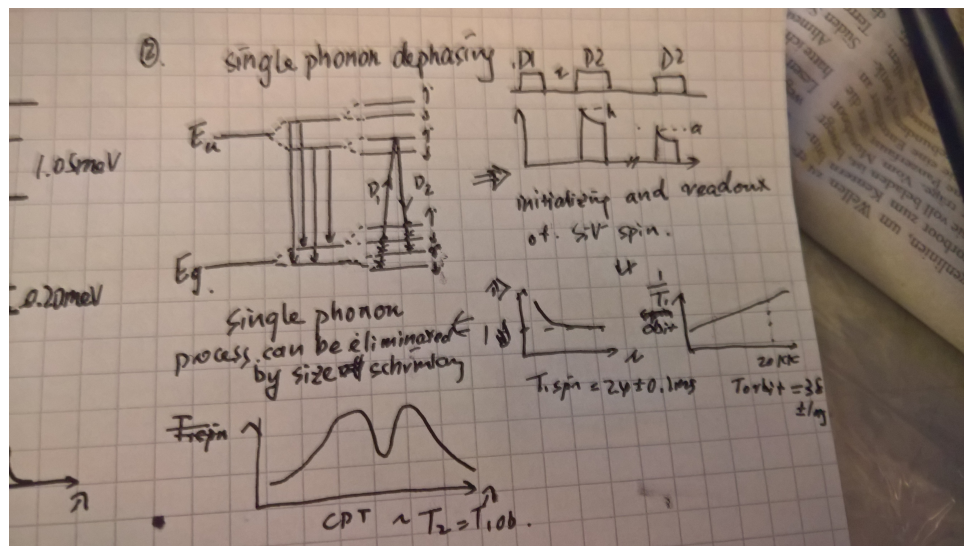


FIGURE 1.2

1.3 Silicon vacancies in nanodiamonds

As mentioned, one vital problem to solve if we want to use SiV^- as a qubit is that, the coherent time has been limited by the rapid orbital relaxation. And this is caused by the transition between the degeneracies of ground

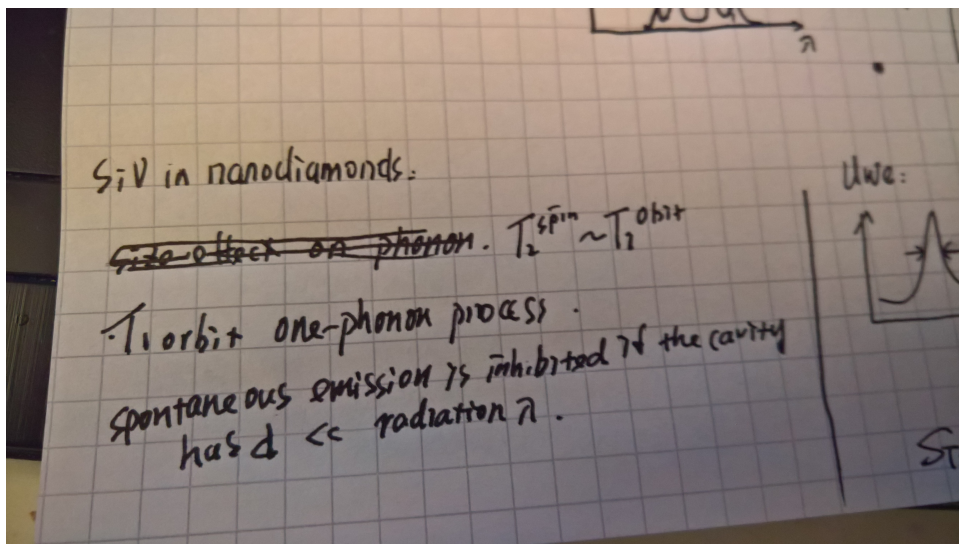


FIGURE 1.3

state which was driven by a single phonon. The elimination of such phonon is an direct approach towards the solution.

Spontaneous emission is inhibited if the cavity has characteristic dimensions which are small compared to the radiation wavelength [Daniel Kleppner 1981]. As in our case to eliminate the emission of phonon that couples into the splitting of ground state in SiV⁻ 47 GHz, nanodiamond of the size that is smaller than the half wavelength of this transition phonon wavelength (around 125nm) is desired.

Currently 3 major techniques are employed in the field of nanodiamond fabrication: denotation, CVD, and HPHT, while the exotic atoms can be mixed in the beginning or implanted via ion implantation. While the denotation method produced highly defective diamonds and ion implantation introduces inner strain, for the SiV containing nanodiamonds, HPHT method and CVD method are the top choices.

The principle of CVD method is to disintegrate the CVD fabricated diamond film, while the HPHT method initialize an phase transition of carbon at high temperature and high pressure. Previously, comparison between the PL spectra of silicon doped polycrystalline diamond films obtained by the CVD method and diamond single crystals grown at a pressure of 6 GPa from a nickel melt at 1500°C has been carried out, and demonstrates that the HPHT diamonds carries narrower SiV⁻ ZPL lines than CVD fabricated ones[C. D. Clark 1995]. As in the department of nanodiamonds, the narrowest SiV⁻ ZPL that has been measured by far, which has a corrected width of 206MHz, that is almost of the excitation state life time limit, is also from the HPHT method fabricated nanodiamond.

1.4 Motivation of the thesis

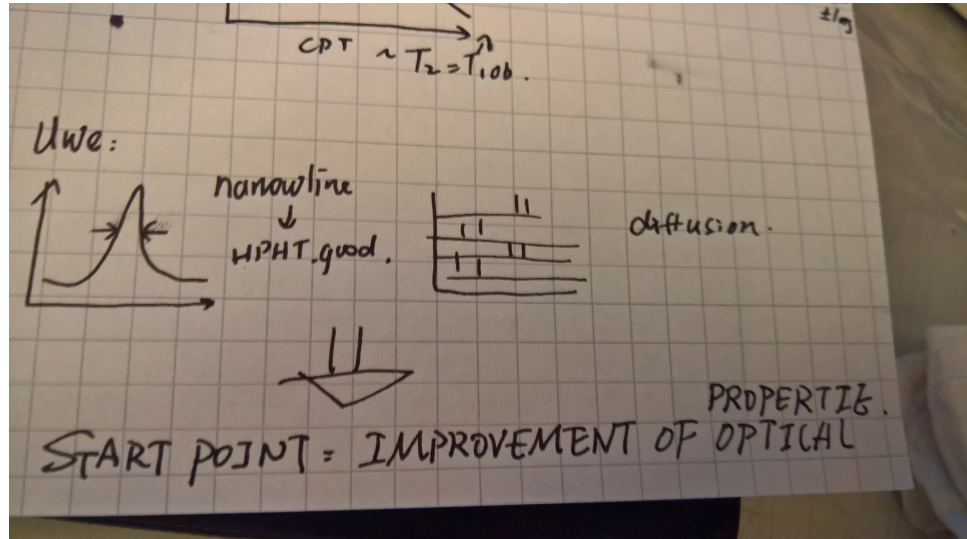


FIGURE 1.4

The motivation of looking into SiV^- in nanodiamonds is to acquire longer coherent time by eliminating the phonon that is responsible for the transition between the fine splitting of the ground state. Yet the obstacle on our way of justifying this approach is that, the optical properties of SiV^- in nanodiamonds are not as outstanding as it is in bulk diamond. Blinking and spectral diffusion, especially spectral diffusion has stopped us from further life time measurement.

The mechanism behind the spectral diffusion is yet not clear, our first guess is to connect the enhancement of spectral diffusion in nanodiamonds with the surface condition, due to the high surface to volume ratio of nanodiamonds.

Our target of this thesis is to improve the optical properties of nanodiamonds, more specifically, to suppress the spectral diffusion via methods of surface treatment, enabling further measurements including but not limited at orbital/spin T_1 and coherent population trapping, and finally to test out the possibility of acquiring a longer coherent time via the elimination of the single phonon process.

In the synthesis procedure of HPHT nanodiamonds, due to the surface absorption of nitrogen on ingredients, NV can be introduced. N atoms act as a n-type dopant, an electron donor in the diamonds. Due to the different dopant density on the surface and in crystal, to match chemical potentials at the surface and in the bulk, charge builds up on the surface depleting the donor charges a depth into the bulk and bending the bands accordingly.

The width of this depletion layer can be calculated with the equation

$$D = \sqrt{\frac{2\psi V(0)}{qN_D}},$$

where ψ is the dielectric constant, $V(0)$ is the band bending and N_D is the concentration of dopant. As in our case, the concentration of Nitrogen is not clear but expected to be low, thus resulting in broader depletion layer. With a typical moderate dopant concentration of $10^{-16}/\text{cm}^3$, the width of depletion layer is calculated to be 80nm[Diederich,1998]. As mentioned before, to inhibit the generation of 47 GHz phonons, the diameter of the diamonds need to be smaller than 125nm, and there is a high chance that

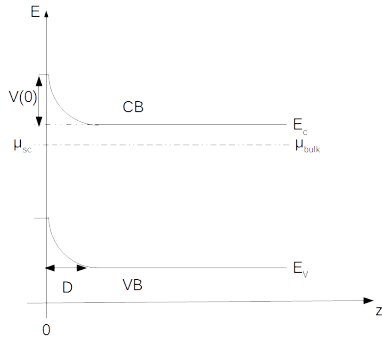


FIGURE 1.5: A sketch describing the band-bending of n-doped diamond. Since the chemical potential of the surface and the doped bulk area need to match up with each other, a depletion layer is formed, the bands (CB: conducting band, VB:valence band) bends towards up near the surface.

SiV in nanodiamonds will lie in side or close to the band bending area, which may be the cause of spectral diffusions.

It is expected to flatten the band bending by inhibit the surface charge accumulation. In this thesis, 2 methods are applied.

First is to remove the graphitic defect by aerobic oxidation. Aerobic oxidation is a good method for surface purification and initialization. Research on denotation diamonds shows that, with the temperature between 375°C to 450°C , the removal of Sp^2 [Osswald,2006]. After 2h of aerobic oxidation at 575°C , the surface structure of HPHT NDs is very similar to bulk single crystals where hydroxyl and possibly ethers are the dominant functional groups[Wolcott 2014]. Aerobic oxidation with elevated temperature can cause the size reduction of nanodiamonds. It has been reported that the average height reduction rate of individual crystals was $10\pm1\text{nm/h}$ at 600°C , $4\pm1\text{nm/h}$ at 550°C and less than 1nm/h at 500°C from aerobic oxidation. Since graphitic defects on the surface of diamond are possible electron trap candidate[J. Ristein, Diamond Relat. Mater. 9, 1129 (2000).], it is possible to lower the surface charge via aerobic oxidation.

The second method is to achieve negative electron affinity via Hydrogen termination, due to the electrostatic effect of the dipole moment p of the heteropolar $\text{C}^- \text{H}^+$ bonds. As most of the reducing agents would rather form different types of hydroxyl groups on the surface than replace the surface groups with C-H bond, only the direct reaction with elemental hydrogen enables the formation of C-H bond as surface termination. Hydrogen plasma has been applied to bulk diamond and diamond thin film as a method to achieve full coverage of hydrogen termination as well as to nanodiamond powers[Yeap Langmuir 2009].

Chapter 2

Sample preparation and Experiment Apparatus

2.1 Sample information

The nanodiamonds that are used as sample in this project was synthesised from a trinary mixture of naphthalene ($C_{10}H_8$), highly fluorinated graphite ($CF_{1.1}$) and Tetrakis(trimethylsilyl)silane($C_{12}H_{36}Si_5$) at a pressure of 8 GPa and a temperature of 1100°C. These nanodiamonds carry optically active SiV and NV. The presence of NV is the result of spontaneous doping from the synthesis procedure, more specific, is due to atmospheric nitrogen adsorbed on the surface of naphthalene powder.

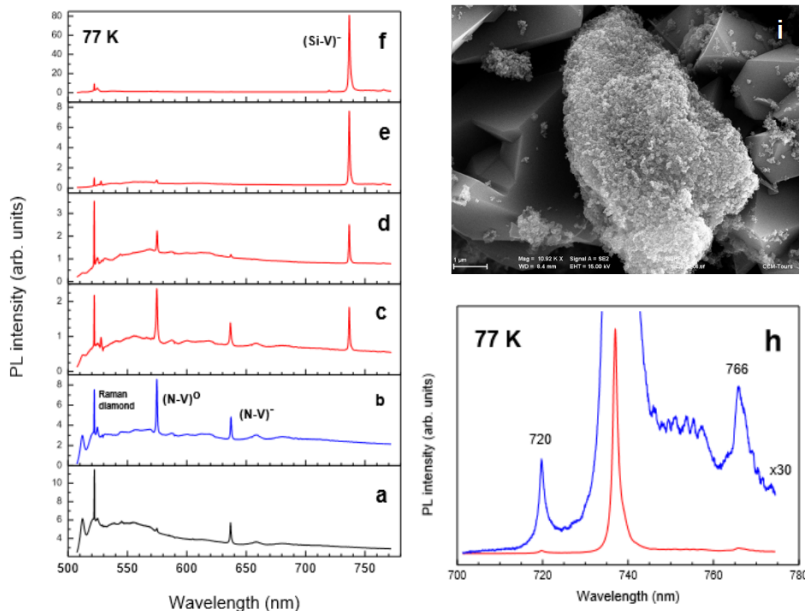


FIGURE 2.1

To obtain cleaner and more size-refined nanodiamond, the sample was then centrifuged and divided into 4 batches following the condition in table 2.1. in between each step, the residue was re-dispersed in 1ml of microwater. The average size of the nanodiamonds in batch 1 is expected to be the smallest, and the ones in the 4th batch are expected to have the largest size.

TABLE 2.1: Centrifuging conditions for nanodiamond size selection

Batch Number	Centrifuging Condition
1	2000rpm 1min
2	1000rpm 1min
3	500rpm 1min
4	300rpm 1min

2.2 sample preparation

2.2.1 preparation of the substrate

IIa diamond as substrate To choose a proper substrate for the nanodiamond sample, a few principles need to be considered.

1. Low background fluorescence. It is always vital to obtain a decent signal to noise ration in any kind of measurements. As for our case, the emission(fluorescence) from silicon centers are the target, thus we would love to lower the back ground fluorescence as much as possilble.
2. Good heat conductivity at low temperature. From previous calculation done by Uwen Jantzen, we know that the temperature difference ΔT between the bottom of the substrate and nanodiamonds(which are spin coated on the surface of the substrate) can be estimate as $\Delta T = \frac{\sigma \cdot d \cdot T^4}{k}$, where σ is the Stefan–Boltzmann constant, d is the thickness of the substrate and k is the thermal conductivity. To resolve the fine feature of silicon vacancy ZPL, we want to characterise the nanodiamond sample at a temperature that is lower than 30K for spectrometer and 10K? for PLE.
3. No distracting spectral features. Some misleading peaks from the emission of the substrate would be the least wanted when we want to character a sample spectrally. In many cases, this is related to the raman-scattering of the photons, which highly depends on the crystal structure of the substrate. This scattering process alters the energy of the incident photons by shifts of concrete values and sometime can introduce peaks that are misleading or distracting.
4. Refractive index. Inam et al calculated the relative emission rate for radiating dipoles near an interface between two dielectrics with FDTD simulation. The result demonstrates that in both of the cases, when the dipole lies perpendicular and parallel to the substrate, the emission rate from a interface with lower relative refractive index is always higher than that from a interface with higher relative refractive index. And to increase the emission rate, a substrate with lower refractive index would be prefered.

Previously, taking these principles into consideration, my collegues have already ruled out a couple of materials, for instance, glass/quartz(distraction

raman shift lines) and Sapphire(also a distracting raman shift line, and impurity induced emission that calls for extra attention when picking the optical filters). Now the temporary choice has landed on IIa type diamond, which has a low impurity density(resulting in low background fluorescence intensity), relatively low refractive index(2,4 to 2,7), good thermal conductivity($\Delta T = 4,17 \cdot 10^{-2} K$) and a raman shift at $1332 cm^{-1}$ that causes no distraction on our observation.

Focused Ion Beam milling In order to make it more convenient to trace the nanodiamonds, markers were curved onto the surface of the IIa type diamond substrate, this work was done by Uwe Jantzen during his master's thesis period. As is shown in the fig.[], the focus ion beam bombards the surface of diamond away and leaves behind markers that are visible in optical microscopy images and SEM images, as well as confocal microscopy images. But the impact of ion may also introduce new defect into the substrate, which will be discussed later.

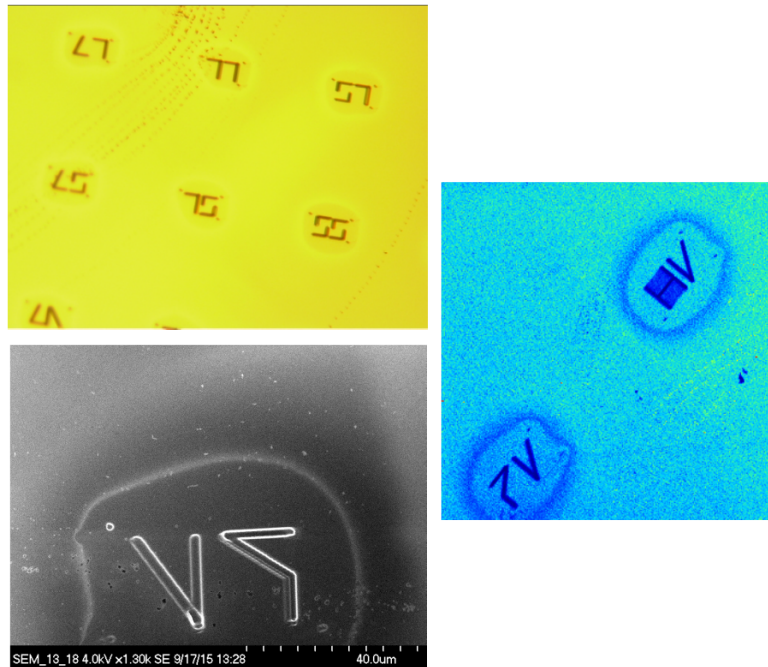


FIGURE 2.2: Pictures of markers obtained from FIB, which are placed following the order of numbers. They are visible in optical microscopes, confocal microscopes as well as SEM

2.2.2 spin-coating of the sample

spin-coating theory

Spin coating is the method of sample preparing that mainly contains 2 steps:

first, the preading of the liquid. In this step, certain volume of liquid containing the particle that we want to coat with is dropped on the surface of the substrate, driven by the centrifuging force from the rotational movement of the substrate, the liquid would be spread evenly on the surface.

Next, the evaporation of the 'solvent'. While the sample stage rotates, the 'solvent' (In our case is not a real solvent, since nanodiamonds never really desolve.) would evaporate, leaving the particle/molecules that are wanted to be coated on the substrate.

In the spin coating session, a few factors we find important.

1. spin speed: generally the thickness of the liquid layer t is proportional to the inverse of the angular velocity w squared $t \sim \frac{1}{\sqrt{\omega}}$, higher speed would help with forming a more uniform layer, yet this also means a smaller volume of solution, which would lead to lower density of nanodiamonds on the surface. On the other hand, with lower speed, the probability of aggregation would increase, which is also what we want to prevent.

2. volume of the 'solution': larger volume means longer drying time, which would increase the probability of aggregation and losing nanodiamonds, while smaller volume leads towards lower density of nanodiamond and more difficulty when trying to drop it with a pipette.

3. type of solvent: The type of solvent, viscosity and boiling point are important for the dispersion of nanoparticles inside solution, the spreading of the solution while spin coating and the rate of evaporation.

4. surface condition of the substrate. High contact angle is an obstacle towards the spreading of the solution, high roughness or inappropriate surface group of the substrate can result in poor wettability from the solution.

Acid cleaning

To make sure that the NDs dispersion can evenly spread and eventually settled on the substrate, a smooth, clean and hydrophilic surface is important.

Acid boiling is a very practical way of diamond substrate cleaning. As it is called, the diamond will be boiled in a mixture of three strong mineral acids: sulfuric acid, nitric acid and perchloric acid. This mixture has very strong ability of oxidizing.

After assembling the setup, we initialize the reaction by heating the mixture to a temperature where it mildly bubbles. The substrate would stay inside the boiling tri-acid mix for 4h. After the acid boiling, the sample should be removed from the flask and rinsed with pure water, after which a rapid blow dry with clean air is compulsory. The mixture of strong mineral oxidizing acid can remove most of the adhesions on the surface of diamond substrate, leaving a clean hydrophilic surface. This oxidizing procedure will lead to the formation of carbonyl and carboxyl groups. One thing that worth notice is that, although via acid boiling, most of the attachments on the surface can be removed, there is still very high chance to introduce other contaminations from the water, and air while the sample is still wet. So a rapid blow dry after the rinse is highly recommended, and if the acid cleaning is not operated in clean room, it is very important to clean the sample a second time via acetone boiling and ultrasonic bath in the clean room.

spin-coating practice

Throughout the project, with the help of Andrea Kurz, several combination of these factors had been tried out on different samples.

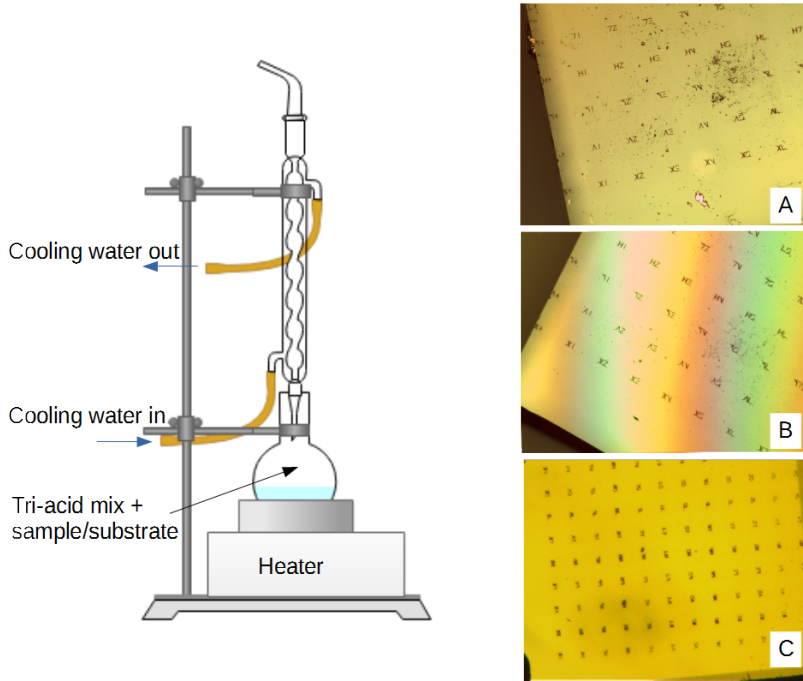


FIGURE 2.3: a) setup up of acid cleaning. b)substrate 207 before cleaning. c) substrate 207 after acid boiling. d) acid cleaned substrate 207 after acetone boiling in the clean room.

I. 35ul Chloroform with 1ul of nanodiamond, take 2ul of this kind of mixture and drop it on the substrate in one time. The spin speed is 5000rpm and the duration is 40s.(Sample 1506,1507)

II. 30ul Chloroform with 1ul of nanodiamond, 2ul of mixture, apply in one time, 5000rpm and 40s.(Sample 1508,1509)

III. 30ul Choloroform and approximately 120ul of water with 1ul of nanodiamond, 2ul of mixture, apply in one time, 8000rpm and 40s.(Operated on substrate207 and found no SiV⁻ signal later.)

IV. 30ul Choloroform and approximately 120ul of water with 1ul of nanodiamond, 10ul of mixture, apply in 5 times, each time 2ul, after each application, spin with the speed of 5000rpm and duration of 40s.(sample 1510,1512)

All the 3 methods other than method III produced samples with SiV⁻ containing points of interest. But among them, the method IV offers the highest SiV⁻ density.

2.3 Experiment Apparatus

The initial Setup

The setup can be coarsely separate into laser source, confocal microscope(with APD and spectrometer as detector), flow cryostat and vaccum pump 4 parts, they are all sketched in Fig. 2.4.

While the absorption spectrum shows the highest off resonance absorption around 530nm[need check need find reference paper], the ZPL of silicon vacancy lies around 737nm. Acknowledged of such information, we

choose to use green laser of wavelength 532nm as the laser source for photoluminescence spectrum and Titan Sapphire laser with the ability of scanning around 737nm as the laser source of photoluminescence excitation. These two methods will be more detailed written about in the following paragraphs. The lasers are coupled into the same photonic crystal fibre, which guides the beam towards the optical table.

The second part is the confocal microscope, which is a very useful tool for imaging of samples that emits fluorescence, such as SiVs. Compared with fluorescence microscope, as sketched in Fig. 2.5, the confocal microscope uses a pair of convex lens and a pinhole that conjugates to the lens to achieve the increase of resolution and signal to noise ration. In the setup, there are two possibilities of signal detection, controlled by a flipping mirror, we can choose to count the photons with a pair of APD, or record the spectrum with a spectrometer. As the resolution of fine splitting of SiV ZPL needs to be measured in low temperature, the motorized sample stage is placed in a flow cryostat, the objective lens is also inside the cryostat. As the name mentioned, the decrease of temperature in this cryostat is achieved by the flow of cold, boiling liquid Helium, a transfer line connects the Helium dewar and the inlet of the helium cooling circulation inside the cryostat. The sample sits right on the cold finger, with proper method of mounting and substrate, the temperature can be brought to as low as 3.5K(need to check).

To reach cryogenic temperature, it is vital to cut off the heat exchange between the sample and the world out side the cryostat, since air and stainless steel(the material of the cryostat wall) can both conduct heat, a UHV condition need to be meet. In our setup, it is realized by the pumping system of a back pump and a turbo pump. The back pump pre-pumps the pressure until it meets the working condition for turbo pump.

Methods for characterisation

With the mentioned setup, we are able to characterise the sample with following basic methods.

Photoluminescence Photoluminescence detects the emission after the absorption of photons. In our case, we use the 532nm laser to excite the sample, which would bring the SiV^- to the second excited state, while the electronic transition between 2 energy levels of the same parity is not allowed, it is possible to conduct the transition between such kind of 2 energy level via the creation and annihilation of phonons, thus it will be the 4 transitions between the first excited state and the ground state that we are expect to record in the spectrum .

The resolving power of a grating in a spectrometer depends on the width of the grating, the centre length to be resolved and the geometry of the use condition. In our setup, a resolution of 16GHz can be achieved, which is capable of observing the 4 line structure in SiV^- ZPL, but not enough to resolve a peak with the width of the lifetime limit.

PLE When PL excites the sample with a laser of single wavelength to obtain the information about multiple emissions, PLE, on the contrary, excites the sample with various wavelength and monitors the photon emission from the side band to characterise a single transition. The resolution of PLE depends on the resolution of laser, with the Matisse Titan-Sapphire laser(linewidth of 50kHz), it allows us to resolve single electronic transmission in SiV^- with life time limited line width, as well as to obtain better signal to noise ratio.

time resolved PL spectra It is very inconvenient monitoring the spectral diffusion in the scale of nm with PLE. To help characterise the spectral diffusing behaviour of SiV^- , we improvised the time-resolved PL spectra. By stacking the sequentially taken spectra in the order of time, we can visualize and estimate the spectral diffusion in a more coarse but convenient way.

Departing from the initial setup, a few alternations have been done during the project, which would be discussed in detail in the following up contents.

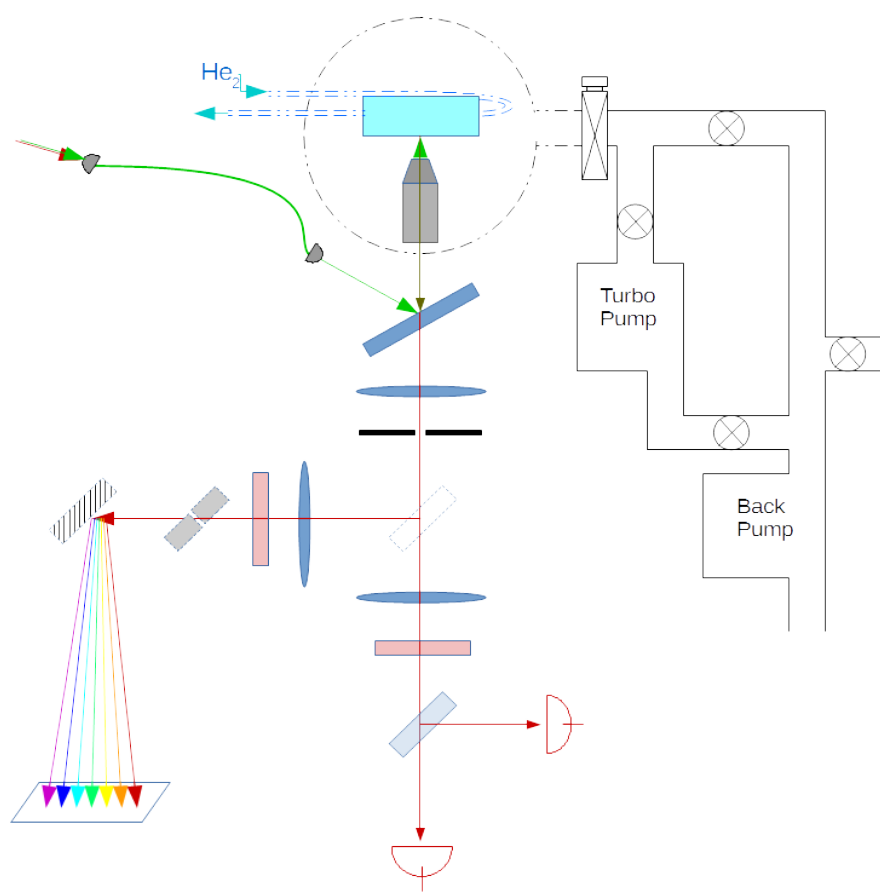


FIGURE 2.4: A sketch of the initial setup.

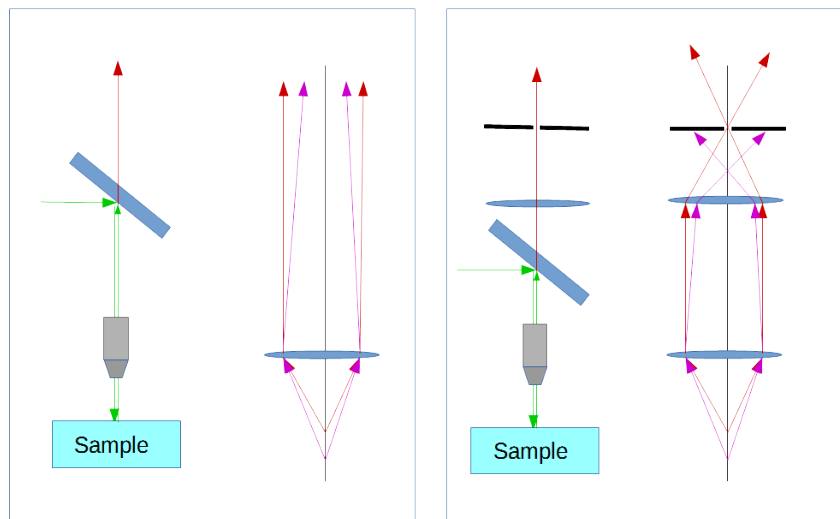


FIGURE 2.5: A)In a typical fluorescence microscope, the back ground fluorescence will also be collected. b)In the confocal microscope, with the help of a lens conjugating pin hole, a large fraction of the fluorescence from non-focus plane will not get through by the pinhole.

Chapter 3

Surface treatments

3.1 Oxidation

Room temperature oxidization is a common way of nanodiamond purification. With different oxidizing temperature, different types of impurities can be removed from the surface of the nanodiamond, ranging from water and physisorbed organic impurities, amorphous carbon, and graphitic shells and ultimate the sp^3 phase of diamond[T.Gaebel,2010]. After the oxidation, carbonyl and carboxyl groups are formed on the surface[Petrakov,2012]. Several paper have mentioned temperature choices for oxidation aiming at impurity removal. During the master's thesis period, 2 different oxidation has been examined.

3.1.1 first Oxidation

As reported, it is possible to achieve the removal of sp^2 carbon without any oxidation on sp^3 carbon via aerobic oxidation with temperature between $375^\circ C$ and $450^\circ C$. With temperature lower than $500^\circ C$, the size reducing rate of nanodiamond is lower than 1nm/h . As our first treatment, we carried out a two step oxidation on sample 1508 and 1509, to achieve the complete removal of graphitic defect on the surface and light oxidation on the surface. Sample 1508 was spin coated with nanodiamond batch2, sample 1509 was spin coated with nanodiamond batch1.

The aerobic oxidation is carried out in a tube furnace and it is done with the help of Markus Mohr. The tube furnace consists of a glass tube connected to the room atmosphere and heating coils around the glass tube. The glass tube can be slide in or out of the heating coils. We put our sample inside a ceramic sample holder and put the holder into the glass tube carefully, after the temperature has been raised to $460^\circ C$, the glass tube was slide into the heating coils. The sample was oxidized at $460^\circ C$ for 90min,then $480^\circ C$ for 40min. After the Oxidation, the glass tube was slide out and the sample stayed inside the tube until it reached room temperature.

Before the oxidation, the samples was first mapped with a room temperature setup that resembles fig. 2.4, but without vaccum pump and cryostat. To make a map of SiV^- containing points of interest, it was first taken, a scan with green laser while the fluorescence was recorded by APD, which offers us a confocal microscopy image of the sample, then the photoluminescence spectra of the bright spots were taken, coordinates of those ones with a sharp peak at 737nm saved as points of interests for the reference of further examine.

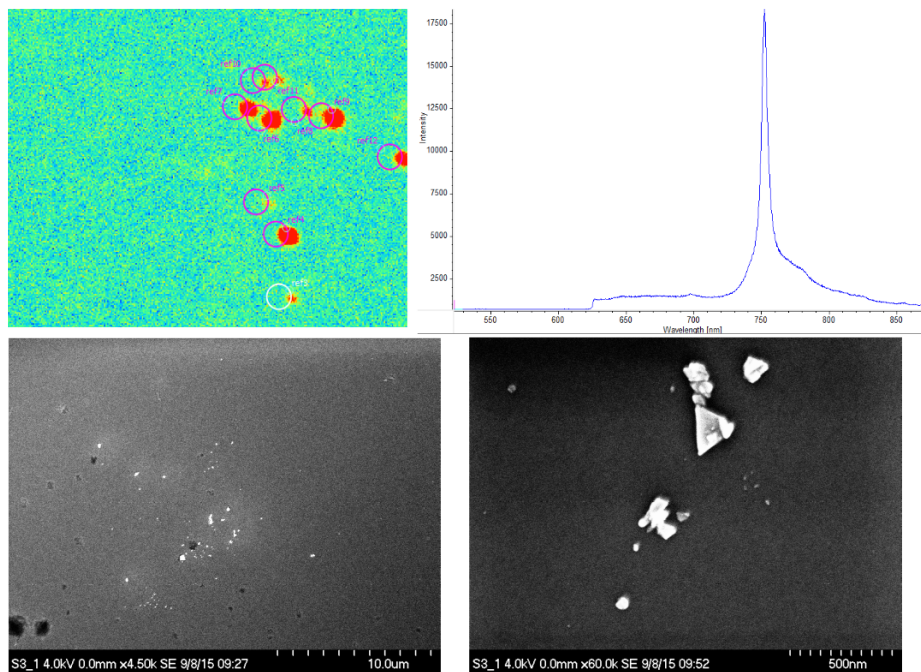


FIGURE 3.1: A)confocal image of a region of interest. The bright spots with circle markers are points of interest. B)Room temperature spectrum of a poi recorded by spectrometer. C)the roi in SEM. D)ref10 and 11 in SEM.

Once the map was acquired, we bring the samples to the electron microscope center and observed the regions of interest with SEM. SEM showed that, sample1508 contains more big single crystals that are larger than 300nm and clusters, while sample 1509 contains more single crystal with under 200nm sizes. This proved that the size selection via centrifuging has worked.

The samples was then attached to an cold finger and the placed inside the cryostat, after UHV condition has been achieved, the helium transfer was started, which would brought the temperature of the sample down to 4.8K. Most of the mapped pois are refound. Excitation with 532nm green laser double checked the existence of SiV. After the confirmation, it has been tried to carry out a resonance excitation with Titan Sapphire laser, when observing a few points of interest next to marker 5A in sample1509, it was noticed that while scanning the red laser across the line with the help of very low amount of 532nm for repopulation, a spectral diffusion of 6GHz in 15Min has been observed. To exclude the possibility of instrumental error, PLE has been operated on the bulk diamond sample with also SiV inside, where no spectral diffusio has been observed(Fig. 3.2). It has also been noticed that the increase of green laser power can cause more severe spectral drift/jump. In a case when the power green laser is brought up for a better refocus, the line has shifted totally out of the range of the spectra scan, and didn't recover in 10min. This observation brought difficulty in the measurement of orbital T1, since we always need to initialize the obital states with green laser, and this spectral diffusion that is related to the application of green laser can result in the fail of hitting the resonant wavelength, since it is technically difficult to refind the line and adjust the wavelength of the resonance laser coordinately.

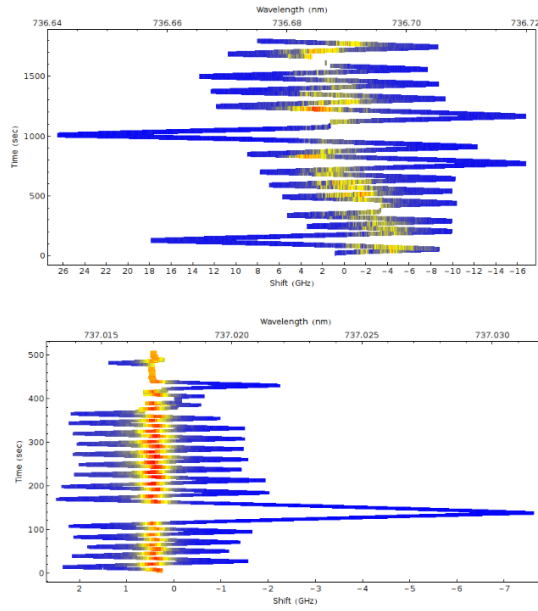


FIGURE 3.2: PLE scan over time on A) ref5A_014 from sample1509 and B) a SiV⁻ site from bulk diamond sample 33b. No significant spectral diffusion been found in bulk diamond sample, which exclude the possibility of instrumental error.

After the obeservation above, we want to study more about this spectral diffusion behaviour that is associated with the green laser. We noticed that the sudden jump/diffusion when more green power is applied can be larger than 20GHz, maybe it is easier to track the movement of the lines with the high resolution grating of spectrometer than with PLE.

To observe the diffusion with a spectrometer, we introduced time-resolved photoluminescen spectrum, which has been described in last chapter. Due to the technical problem, our motorized sample stage can not move ideally in the vertical direction anymore, which has limited our region of observation. This time we refound the ROI around the marker 4C. And recorded the time-resolved spectrum. A session is set to be 60 spectra taken consecutively. At first, to feel the long term diffusing better, 3 sessions, with a refocus after each, are undergone for each points of interests. Since line diffusion in PLE gets wider when raising the green laser power, we excite the sample with 500uW power in front of the objective lens to obtain more diffusion. As a result, line diffusion up to 1nm has been observed. Sequentially we decrease the input power to examine the power dependency of spectral

Taking the samples out of the furnace, we noticed that the surfaces of the

samples turned very dirty. It is yet not clear, what the contaminations are, are they intrinsic or are they extrinsic. A possible explanation is that, the contamination comes from the glass tube of tube furnace, that the residues of previous treatments has attached to the inner surface of the tube and evaporized again, depositing on the surface of our sample. Further improvement of oxidation operation has been done in our second oxidation test, and will be mentioned in the next part of the thesis.

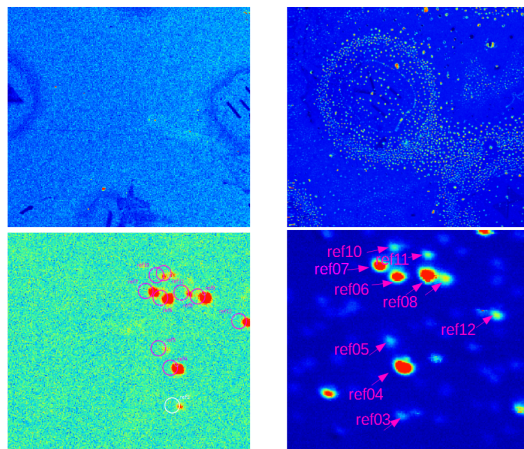


FIGURE 3.3: A) region of interest next to marker 3C of sample 1508 before oxidation B)the same region of interest after oxidation C) Points of interest from the ROI before oxidation D)points of interest after oxidation

After the oxidation, both of the samples showed very bright background. In sample 1508, large amount of bright spots around the markers has been found. They are not SiV or NV, and will bleach away very fast once been focused on.

I couldn't re-find any marker from sample 1509 due to the large amount of fluorescence from the surface. For sample 1508, the region of interest next to marker 3C was still visible, despite all the disturbing bright spot next to it.

Sample 1509(substrate 207) was then acid cleaned, at the same time sample 1508 was moved into the cryostat, time resolved spectra were recorded. After the oxidation, we learned that the beam polarisation is not conserved within the photonic fibre, so that a polarising beam splitter and a liquid crystal noise eater was added after the fibre to obtain steadily vertically polarised beam. Using the same method as before oxidation, time-resolved PL spectra was recorded.

3.1.2 second Oxidation

The surface function groups play very important role regarding the surface charging state. It is interested to observe, the spectral behaviour of SiV in nanodiamonds, when the surface is initialized the same as bulk diamond. As reported in [Wolcott 2014], after 2 hours of aerobatic oxidation at 575°C , the surface structure of HPHT NDs is very similar to bulk single crystals where hydroxyl and possibly ethers are the dominant functional groups. It is also interesting, since the elevated oxidation temperature can

reduce the size of nanodiamond, to observe the behaviour change as the SiVs will be even closer to the surface after oxidation. Sample 1510 was prepared for this treatment, nanodiamond from batch1 was spin coated on the substrate186_1 with method IV.

We tried to spin coat substrate 207 at the same time, but failed. The droplet of liquid refuse to spread over the surface while spinning, we suspect the surface of substrate has been damaged in our last oxidation session, which may result in a higher surface roughness that leads to poor wettability.

Taking the experiences of last oxidation into consideration. This time we introduced inert gas (helium) flow to flush away the potential contaminations during the cooling process. This can also prevent the result to be affected by the humidity of the air. We found out the extinction rate of polarising beam splitter was not ideal for 532nm, so this time we used a Clan Thompson polarisation filter instead.

As mentioned, the polarisation of the beam was not fixed in the measurement before the first oxidation, and while comparing the before and after oxidation spectra, we noticed that, even when the 2 sets of spectra are from the same poi, the spectra pattern can be very different. This made me wonder, if the polarisation of excitation beam has anything to do with the spectral diffusion. To figure this out, we measured the time-resolved PL spectra on 3 pois with different excitation beam polarisation at 4.7K.

The excitation polarisation pattern of other pois are also recorded, but due to low time and Helium budget, it was not affordable to record time resolved excitation polarisation for each of them. Time-resolved PL was later recorded at 20K.

After the oxidation, it was noticed that the sample looks much cleaner than last time. The confocal observation confirmed that, no bright dots like the ones from sample1508 has been seen. The increase of background fluorescence was observed again. Cold spectra showed the existence of GR1 center everywhere.

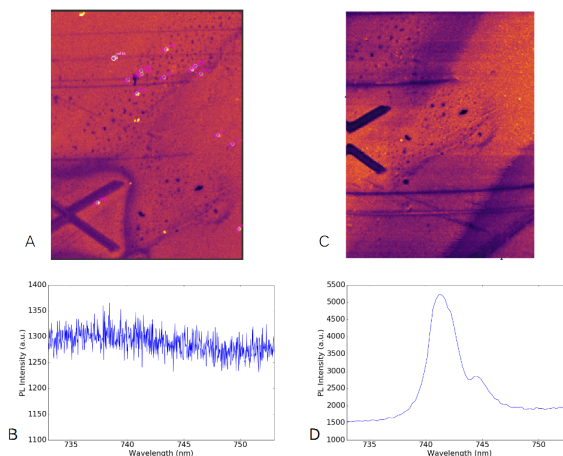


FIGURE 3.4: A: roi before oxidation, pois are mapped. B:Background spectrum of the region, no strong Gr1. C:roi after oxidation, strong background fluorescence, can't find pois. D:Spectrum after oxidation, strong GR1 center everywhere.

I noticed the intensity of GR1 fluorescence is stronger around the FIB made markers. As GR1 centre is a isolated vacancy inside diamond, it is reasonable to suspect that, the impact of focused ion beam may have caused serial collision and collision-induced dislocation inside diamond, resulting in the formation of GR1 centre. The fact that the intensity of GR1 centre is higher after the oxidation can also be explained by this theory, since the cross section is usually of the shape of a droplet, which is larger a few nm beneath the surface than on the surface.

3.2 H termination

As we discussed before, the origin of the band bending is that, the chemical potential of the surface and the bulk region need to match each other, while this adjustment changes the density of charges inside the diamond, it stimulates the generation of space charge, which need to be compensated by the surface charge that is compatible with the shift of the Fermi level from the charge neutrality level (CNL) of the surface state system. The hydrogenate of the diamond surface covers the surface with an atomic layer of C^+H^+ dipole, which lowers the surface potential, switches the surface from PEA to NEA. It has been experimentally proved that Hydrogenated n-doped diamond has flatter band bending than dehydrogenated ones.[Diederich,1998]

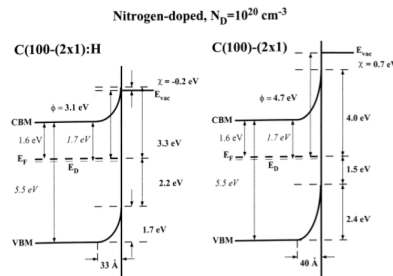


FIGURE 3.5: Band structure of N-doped diamond, due to the shift of surface chemical potential, Hydrogenated diamond has flatter band bending than dehydrogenated diamond.[Diederich,1998]

The surface termination is carried out in a microwave plasma reactor. This is operated by Dr. Christian Osterkamp. We used the same parameters for bulk diamond, (ASK OSCHDI). In [Yeap, 2009], the reaction lasted 60min to maximize the coverage, in our case, considering the low density of nanodiamond on the substrate, we applied the same amount of time as bulk diamond, as the nanodiamond can already be 'dipped' into the plasma thoroughly. The sample that has been used is sample 1512. Sample 1512 was produced by spin coating nanodiamond batch1 on the substrate 186_2, with method IV.

To prevent introducing contamination into the plasma reactor, no characterisation has been done before the termination. The plasma reactor has the similar vacuum system as a conventional electron microscope, the sample was first put into a pre-vacuum chamber then send into the reaction chamber. The shape of the plasma is controlled by a quartz waveguide.

After the termination, we put the sample directly into the cryostat, very high density of SiV has been found and marked. It has been recorded as before, the excitation polarisation pattern and the time-resolved PL spectra.

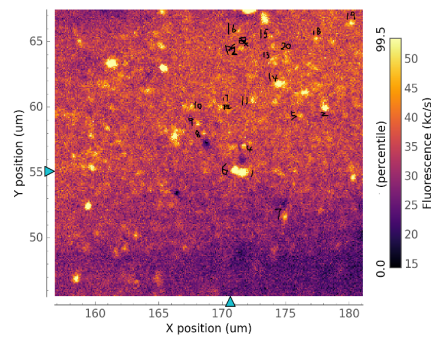


FIGURE 3.6: Very high density of SiV has been found in sample 1512

Chapter 4

Result and Discussion

4.1 Compilation of data

To investigate the spectral diffusion behaviour, recorded time-resolved spectra for each of the POI before and after treatment. After the first oxidation, for better characterisation, time-resolved spectra are measured not only with one but multiple excitation polarisation. This leaves large amount of spectra files (almost 32,000 spectra!), besides visualizing the movement of lines into color maps, we need better tools to evaluate the spectral stability, a way to compile dozens, sometimes even hundreds of spectra into one single value that represents the spectral stability of a POI.

Normalized cross-correlation evaluates the similarity between 2 patterns, the closer to 1, the higher the similarity. Here we compare the time-resolved PL spectra from every time tick with the first spectrum, the average value of this series of normalized cross-correlation reflects the general level of spectral stability of the measured point.

4.2 Nanodiamond size and spectral stability

The observation of nanodiamond with SEM [fig.] fits the expectation, that after the centrifuging size selection, batch1 contains smaller nanodiamonds than batch2. When comparing the time-resolved spectra from sample1508 and sample1510, which were taken at 4K, with an excitation power of $120 \pm 10 \mu\text{W}$, it can be observed that the spectra from sample1510 shows more spectral diffusion. The calculation of mean normalized cross-correlation confirmed the observation. As plotted in the histogram 4.7, the distribution of mean normalized cross-correlation nanodiamond from batch1 is much closer to 1 than from nanodiamond batch2.

As discussed in Chapter 1, in nitrogen doped diamond, to match up the chemical potential inside the diamond and on the surface, a depletion layer was formed beneath the surface, where the valence band and conducting band are bended towards up. The width of the depletion layer differs by the concentration of the donor and is around 80nm in moderately doped diamond ($N_D = 10^{-16}/\text{cm}^3$)[Diederich,1998].

Since the donor level of nitrogen is rather deep (1.7eV) below the minimum of conduction band, it is very hard to thermally ionize the donors at low temperature, but with the excitation of 532nm(2.33eV) green laser, it is possible to excite the electrons from the donor level to the conduction band.

So in our case, there is higher chance for nanodiamonds from batch1, which are of smaller sizes, to obtain SiV^- 's sitting inside the bended band than those ones of larger diameters, like the ones from batch2. For more

information I looked up the position of SiV⁻s in the paper [Rogers2013], where SiV⁻s in bulk diamond are reported to have very good long term spectral stability (no spectral position variation in 90min), interestingly, the distance of SiV⁻s from the surface is larger than 2um, which means they sat in the bulk diamond region instead of band bended region.

4.3 Excitation power and spectral stability

Sample 1508 was excited with decreasing excitation power. The left column of 4.6 shows the changes of time-resolved spectra of POI ref11, the most obviously diffusing line is the one between 738nm and 739nm, whose spectral position changed almost 1nm in 300s. As the excitation power decreases, the diffusion become less intense.

The result of cross correlation is can be seen in ??, where each dot represents a POI in the sample. As shown in the figure, the general level of spectral diffusion decreases as the excitation power decreases.

As I try to explain the spectral behaviour with the band bending layer, the power dependency of spectral diffusion can be explained by the photon induced charge transfer between the conducting band and the surface, which will enhance the band bending, thus with higher excitation power, comes greater spectral diffusion. It is also shown in the figure, that after the oxidation, the response from the spectral diffusion towards the excitation power change is much greater, this gives evidence for the explanation of next observation: temperature change against spectral diffusion, which will be discussed in the next section.

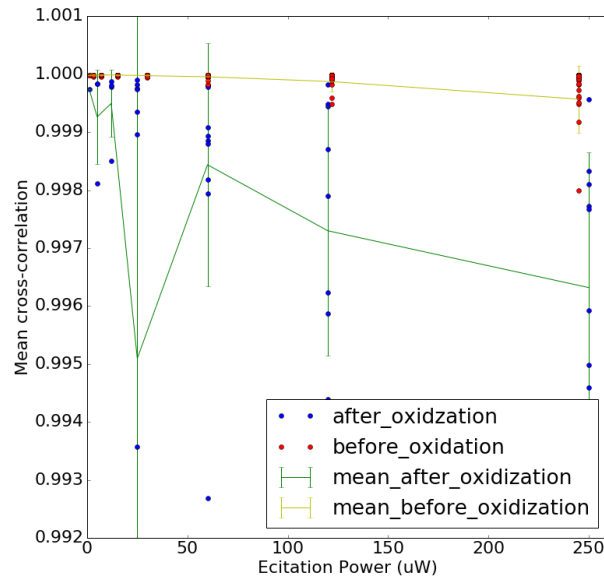


FIGURE 4.1: Powerdependency of nanodiamond batch2, before and after first oxidation.

4.4 Temperature and spectral stability

Comparing the mean normalized cross-correlation of sample 1510 from 4.7K and 20K in 4.7, no significant difference between the two temperatures has been found, which fits the expectation. Since the assumption is that, the donors are ionized with the help of laser, the band bending should stay the same as long as the excitation power is not changed, so shall the spectral diffusion. I consider this result not solid enough as only 3 points were measured for the 4.7K measurement. But it would be interesting to collect more data to justify the prediction.

4.5 Excitation polarisation and spectral stability

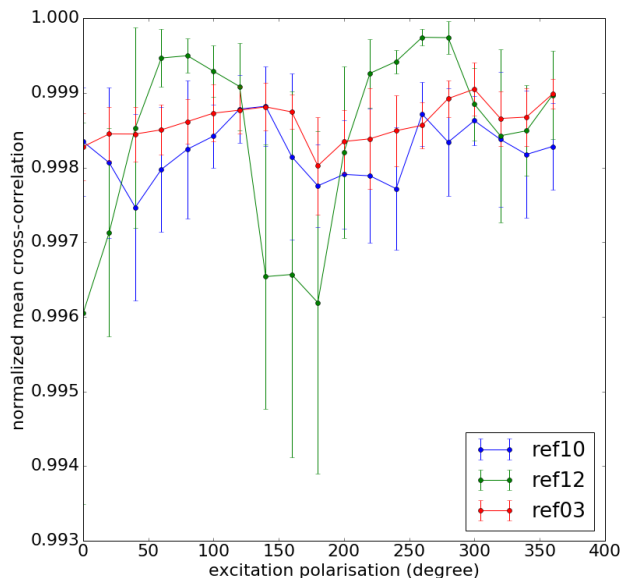


FIGURE 4.2: Mean normalized cross-correlation against excitation polarisation. The error bar stand for standard deviation

The polarisation of photoluminescence has been measured in [L.J.Lachlan,2014], where the excitation polarisation patterns suggested that the SiV⁻ is aligned along the <111> axis of diamond crystal. A set of dots of none-polarisation dependency(excite from the z axis of the SiV⁻), or symmetric patterns that are rotationally separate from each other by an angle of 60° with population contrast of 60% are expected to be observed when excite the SiV⁻ along crystal axis <111>. The polarisation pattern generated from other orientations can be considered as shadowing the <111> axis from respective angle.

In the measurement of excitation polarisation on sample 1510, time-resolved PL spectra are taken with different excitation polarisations. We do noticed some POIs behaved differently when excited with different beam

polarisation^{4.4}. But no clear polarisation pattern has been acquired. Further cross-correlation calculation ^{4.2} showed polarisation dependency like pattern in poi ref12, while the other two pois have no clear pattern.

Further excitation polarisation-resolved spectra were taken on the same sample. In some of the spectra, polarisation-related periodic pattern can be seen on some of the lines, while the sum up pattern give no polarisation dependency.

4.6 Aerobic Oxidation and Spectral stability

The initial target for aerobic oxidation is to selectively remove graphitic defects(the first oxidation) and to generate bulk diamond-like surfaces(the second oxidation). The second oxidation, which was operated on sample 1510, didn't turn out as we wishes, offering no useful data on SiV⁻. The first oxidation on sample1508 and 1509 introduced dark spots that are visible in optical microscopy images, and very bright spots containing no SiV⁻ signal in confocal measurements. Yet it was managed to re-find some of the pois from sample1508.

The aerobic oxidation has greatly enhanced the photoluminescence of the sample in general, including SiV⁻ and background. Before the oxidation, the peak height from PL spectra

4.7 Hydrogen termination

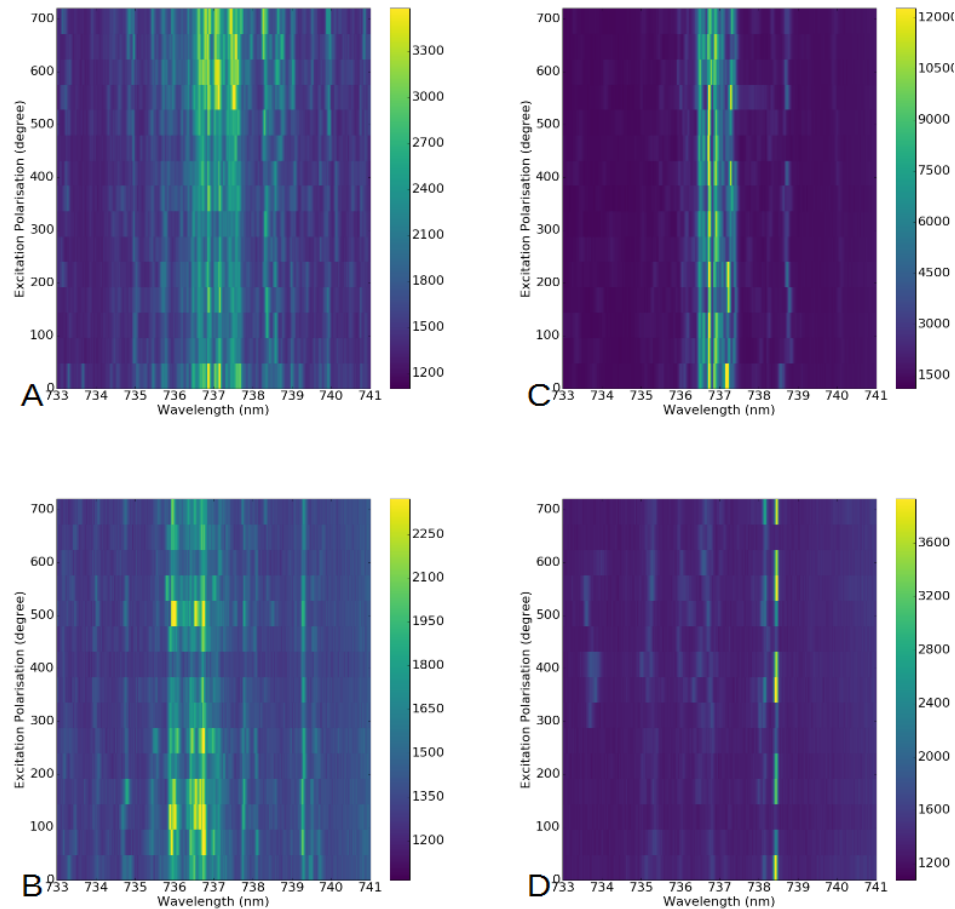


FIGURE 4.3: 4 Excitation polarisation-resolved spectra from sample 1510, A: ref16, B:ref13, C:ref15, D:ref12. Some of the lines in these spectra show polarisation dependency, most significantly can be seen in ref12

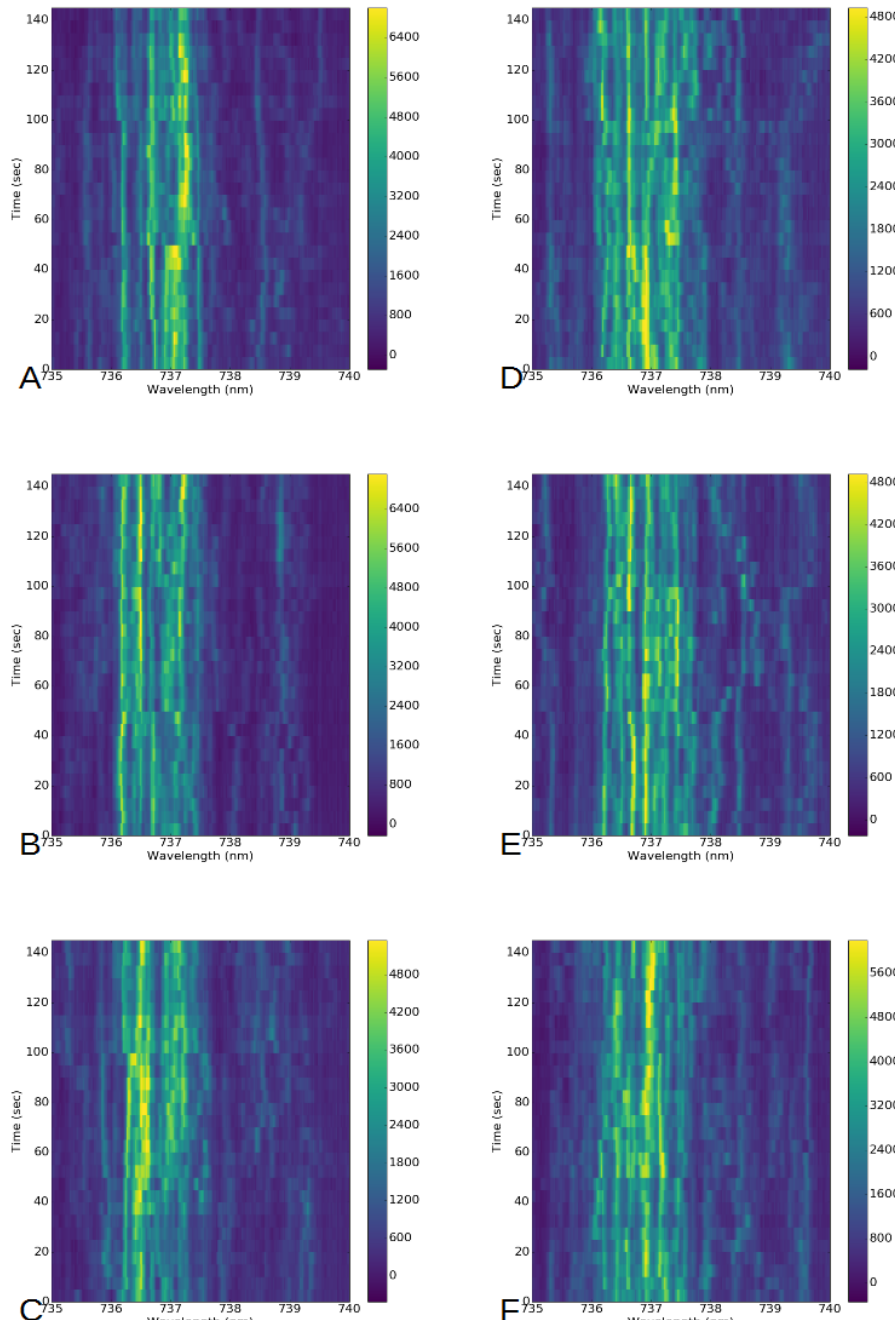


FIGURE 4.4: Time-resolved spectra of poi ref03, sample1510 with different excitation polarisation. Polarisation of the excitation beam: A: 0° , B: 40° , C: 80° , D: 120° , E: 160° , F: 200° .

This figure continues in 4.5

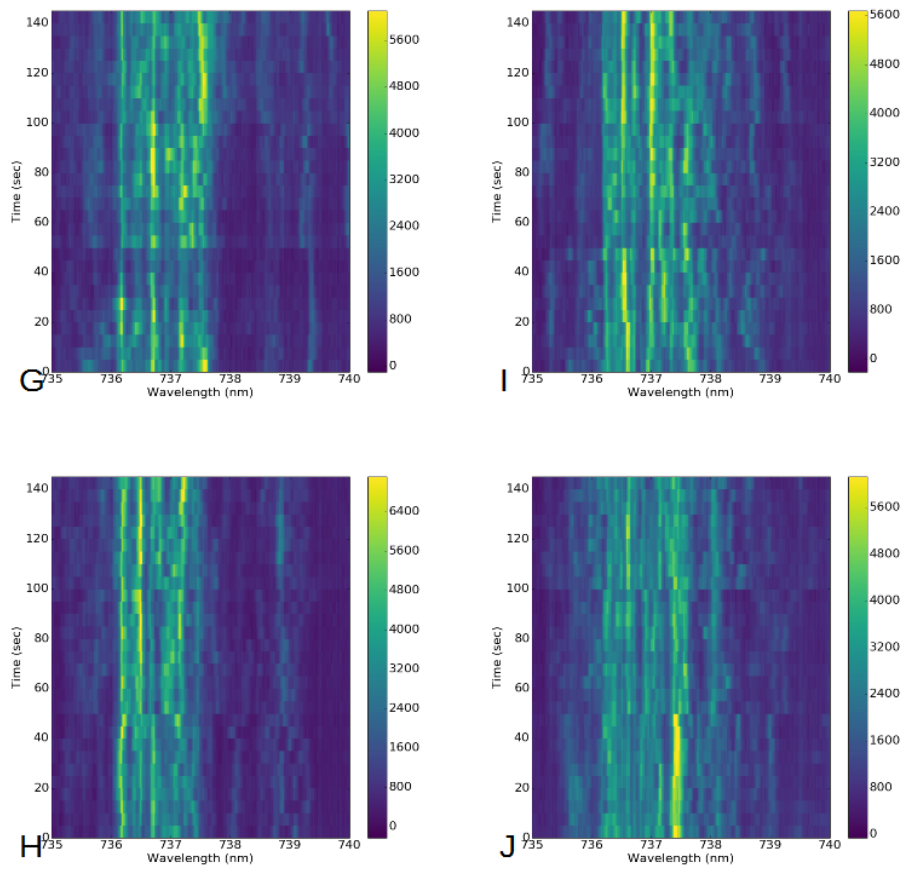


FIGURE 4.5: This figure follows 4.4. Excitation Polarisation:
G: 240° , H: 280° , I: 320° , J: 360°

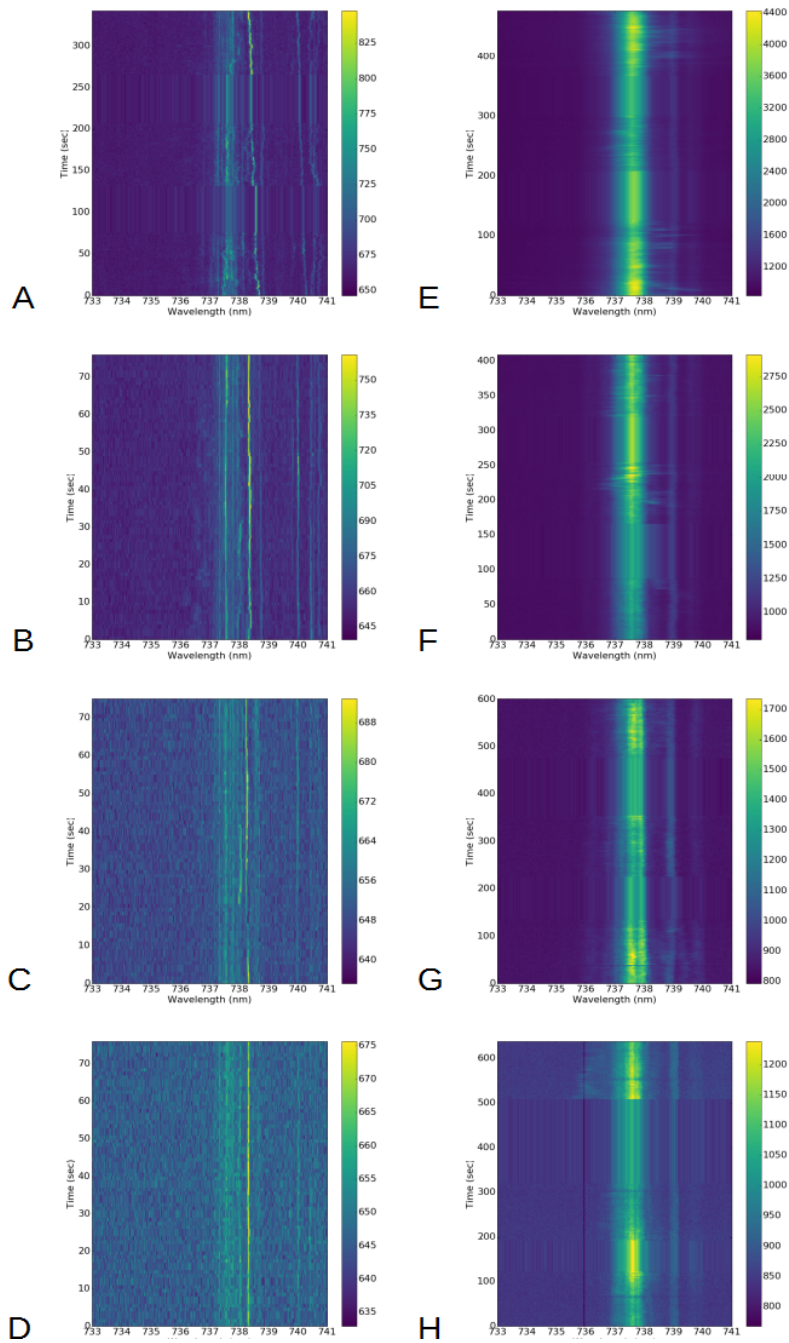


FIGURE 4.6: Left column: time resolved PL spectra of point ref11, sample1508 before the first aerobic oxidation with different excitation power (A:250uW, B:122uW, C:60uW, D:30uW). Right column:time resolved PL spectra of point ref11, sample1508 after the first aerobic oxidation with different excitation power (A:250uW, B:120uW, C:60uW, D:25uW).

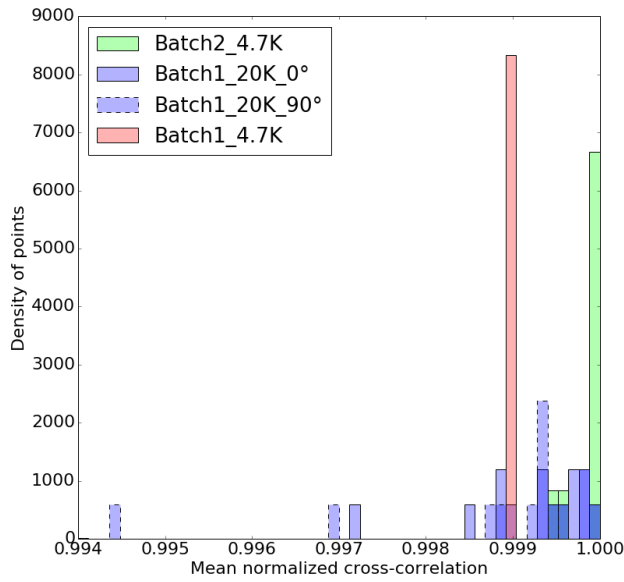


FIGURE 4.7: Histogram comparing the normalized mean value of cross-correlation between untreated sample 1508 (nanodiamond batch2) at 4.7K and sample 1510(nanodiamond batch1) at 4.7K and 20K. The height of the bars are normalized by the integration over bins. The time resolved spectra of sample 1510 was recorded with 2 different excitation polarisation, they are separated with solid and dashed lines.

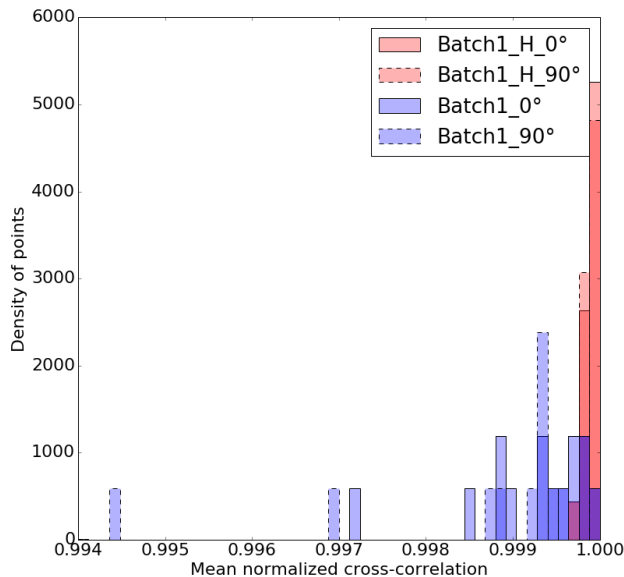


FIGURE 4.8: Histogram comparing the normalized mean value of cross-correlation between untreated sample 1510 and hydrogen plasma treated sample 1512 (both spin coated with nanodiamond from the batch1).The height of the bars are normalized by the integration over bins.

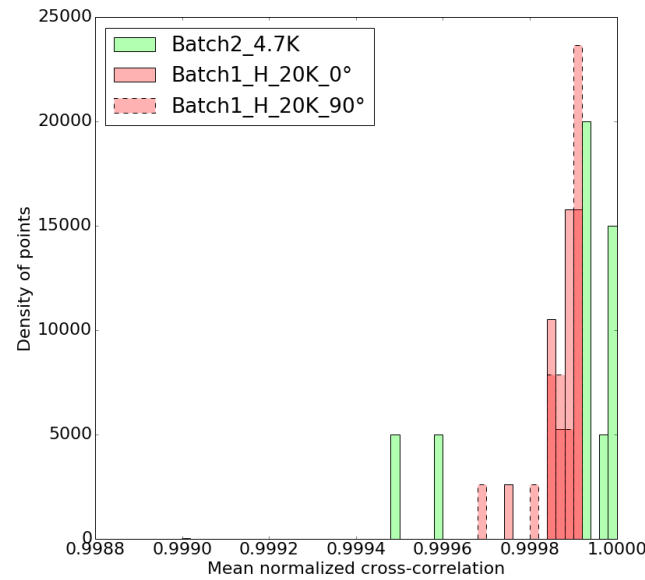


FIGURE 4.9: Histogram comparing the normalized mean value of cross-correlation between untreated sample 1508(nanodiamond batch2) and hydrogen plasma treated sample 1512(nanodiamond batch1).The height of the bars are normalized by the integration over bins.

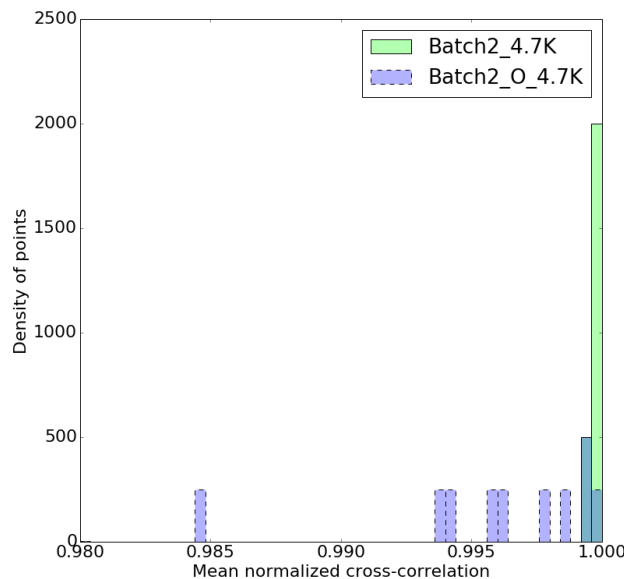


FIGURE 4.10: Histogram comparing the normalized mean value of cross-correlation between untreated and oxidized sample 1509(nanodiamond batch1) at 4.7K. The height of the bars are normalized by the integration over bins.

Chapter 5

Conclusion and outlook

5.1 The road so far

Initial motivation

Development of a method to estimate the spectral diffusion

Surface treatments and their effects

5.2 Probabilities in the near future

PLE

life time measurement

comparasion of different surface group -OH and graphitic patch

better method for size selection porous/gel system, chromatographic way of size selection

relation between surface geometry and spectral behaviour

Appendix A

Appendix Title Here

Write your Appendix content here.